Geometry-Based V2V Channel Modeling over Millimeter-Wave in Highway Scenarios

Yekaterina Sadovaya, Dmitrii Solomitckii, Wei Mao, Oner Orhan, Hosein Nikopour, Shilpa Talwar, Sergey Andreev, and Yevgeni Koucheryavy

***Abstract*—As of today, millimeter-wave (mmWave) bands are employed as part of the emerging 5G technology to provide high data rates for vehicle-to-vehicle (V2V) communications. However, V2V channels over mmWave have not been well studied as of yet due to the complexity of measurements, especially if there is a need to estimate the contribution of adjacent interfering vehicular transceivers. Moreover, the channel models that are currently in use consider vehicles on the road according to a certain distribution, which may not be accurate in practice. Also, past models do not take into account the effects of reflection, diffraction, and transmission through obstacles, as well as the physical properties of vehicles themselves. In this paper, using geometric ray-based simulations, in which the aforementioned effects are incorporated, we present mmWave V2V channel modeling for a highway scenario at 28 and 72 GHz carrier frequencies with both low and high density of vehicles. Our results include such characteristics as path loss, fading, root-mean-square (RMS) delay spread, and angular spread.**

***Index Terms*—Vehicle-to-vehicle communications, Millimeter waves, Radio propagation, Channel modeling**

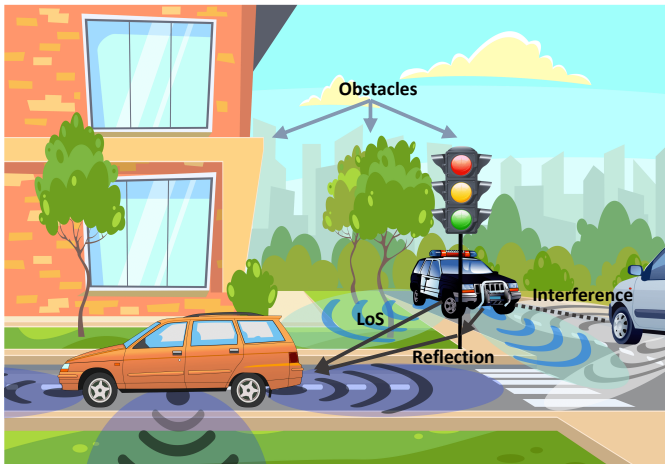

Fig. 1. Signal propagation between moving vehicles.

I. Introduction

According to data from the World Health Organization [1], about 1.35 million people worldwide die each year as a result of road traffic accidents. This horrendous number is comparable to the population of large cities. One of the solutions to increase road safety is to establish communication between vehicles and to improve sensing data exchange from LIDARs and cameras. This allows to steer cars without drivers and create a better monitoring of ambient traffic that can help provide see-through vision and detect hidden objects on the roads [2]. The existing IEEE 802.11p standard is aimed for V2V communication, which operates at 5.9 GHz and can provide the data rates up to 27 Mbps. However, combining advanced sensing data in real-time requires much higher rates on the order of Gbps [3].

Theoretically, 5G provides the data rates of up to 10 Gbps with mmWave extensions. Unlike lower frequencies, mmWave bands have higher reflectivity, and they are also more susceptible to blockage. These properties spawn a new wave of research related to mmWave propagation. Besides this, precipitation and weather conditions have an impact on mmWave propagation. However, in the context of V2V communication, the impact is negligible due to short distances between transceivers [4]. At this point, the question remains of how to characterize a V2V channel in the mentioned conditions by taking into account the considered physical properties as it is shown in Fig. 1.

At the same time, there is insufficient literature on this subject because arranging measurements in the case of mmWave V2V channel is challenging. In [5], measurements were conducted at 6.75, 30, 60, and 73 GHz frequency bands via ultra-wideband (UWB) multi-channel sounder for urban and highway scenarios to investigate the effect of blockage between transmitting and receiving vehicles. However, consideration of two vehicles and a blocker does not account for the interference effects. There are also several works [6], [7] where measurements were carried out with the purpose of determining a relevant antenna position on a vehicle, which allows to estimate the line-of-sight (LoS) path loss (PL) but assessment of any other physical effects was not attempted.

Theoretical V2V channel models have been proposed by the METIS project [8] and other authors in [9]–[11]. All these works consider a stochastic channel model, which implies a deterministic distribution that may not always be achieved in real life [12]. Despite the lack of results related to mmWave V2V channel, there are many studies related to the microwave range for IEEE 802.11p. Measurements via a channel sounder with the bandwidth of 50 MHz at 5 GHz carrier frequency with 20 ns delay resolution were conducted in [13] to contribute an appropriate approximation model. In [14], measurements via a

This work was supported in part by Intel Corporation and in part by RAAS Connectivity RTF framework.

Y. Sadovaya, D. Solomitckii, S. Andreev, and Y. Koucheryavy are with Tampere University, (e-mail: firstname.lastname@tuni.fi), Tampere, Finland.

W. Mao, O. Orhan, H. Nikopour, and S. Talwar are with Intel Corporation, (e-mail: firstname.lastname@intel.com), Santa Clara, CA, USA.

channel sounder were presented at the carrier frequency of 5.6 GHz. In several studies [15], [16], measurements were carried out at 5.3 GHz via 4x30 MIMO system. Measurements and modeling were also conducted in different environments at 5.2 GHz band in [17]. The work in [18] was dedicated to studying signal propagation at 5.9 GHz.

Summarizing this literature review, a gap can be identified in the following way. Measurements over mmWave V2V channel are based on LoS or one-blocker scenarios. In that case, the effect of interference from adjacent vehicles is not taken into account. Theoretical models assume that vehicles follow a certain predetermined distribution. In this work, we characterize mmWave V2V channels by using our custom ray-launching (RL) simulator, which allows to consider the relevant signal propagation effects and physical properties of the environment. Our RL tool incorporates the essential models, which are intended for site-specific deterministic scenarios. The sufficient accuracy of our RL tool was demonstrated in [19], [20]. The main contributions of this work are the following:

- In our simulations, we address a site-specific highway scenario where vehicles do not follow any certain distribution, which is closer to reality according to [12].
- For this scenario, we propose a method to characterize mmWave V2V channels using a RL simulator, which allows to take into account such signal propagation effects as reflection, diffraction, transmission through obstacles, and diffuse scattering, as well as physical properties of vehicles.
- Using the described scenario and approach, we provide parameters for mmWave V2V channel modeling. We also present a comparison of the obtained parameters with the reference results for microwave frequencies. These parameters are useful for further system design, link layer analysis, and beam management optimization.

The rest of the text is organized as follows. Section II describes the approach in use for the calculations as well as the modeling scenarios. Section III outlines the methodology for obtaining channel characteristics. Section IV reports the simulation results. Section V is dedicated to a comparison of our simulation output with the results produced by other authors. Conclusions are made in Section VI.

II. Scenario and Approach

A. Deployment

We consider a 700x15 m highway area with the size of each car 5x2 m, where the length of the highway was chosen as follows. According to the research in [21], one mmWave transiver cannot cover the radius of more than 200 m, since in this case the received signal is equivalent to the noise level. To take into account such cases, the length of the highway must be greater than 200 m. Two scenarios with different vehicle densities were considered. The minimum distance between the vehicles is 1 m. The height of antennas, which are located in the front, rear, and sides of the vehicles, is 0.35 m. Fig. 2 illustrates the deployment of interest. We placed antennas on the bumpers to increase the number of reflected paths, since high reflectivity is one of the properties of mmWave propagation. The considered deployment specifications are listed in Table I.

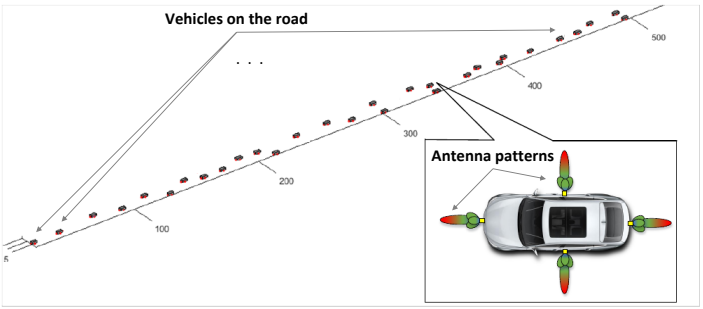

Fig. 2. Vehicular deployment of interest.

TABLE I
Scenario properties

Scenario no.	No. of vehicles	No. of antennas	Density, m^{-2}	Highway size, m
Scenario 1	42	168	0.04	700x15
Scenario 2	106	424	0.01	700x15

B. Ray-Launching

We employed our RL simulator to obtain the required parameters, such as power, azimuth, as well as elevation angle of arrival (AoA), and angle of departure (AoD). The calculation process in our RL simulator is divided into 4 parts. In the first one, verification and conversion of the input data, which consists of geometrical and physical components, are produced. In the second part, the image method is applied to calculate all of the possible multipath components between the transmitter (Tx) and the receiver (Rx). During the calculation, we consider such effects as reflection, diffraction, transmission through obstructive vehicles, and diffuse scattering. Further, electric and magnetic fields are captured by the geometrical optics (GO) and the uniform theory of diffraction (UTD).

The main goal of using this RL simulator is to estimate the contribution of different paths to the total amount of power and thus the PL in two extreme cases: when the summation is done coherently and incoherently. The first option reflects the situation where the Rx may resolve the arriving multipath component (MPC) due to larger bandwidth available. In contrast, the incoherent case is related to the Rx, which is not able to resolve the MPCs. It is worth mentioning that the number of paths in our simulation is limited to 20 for each transceiver.

III. Methodology

A. Path Loss

In our simulations, we consider two situations. The first one is when there is larger bandwidth at our disposal and the sec-

ond one is when the bandwidth is small. These situations refer to wideband and narrowband Rx, where the term narrowband reflects the bandwidth of less than 25 kHz according to ETSI [22]. It makes sense to consider these two cases as they may have different applications. The advantage of a narrowband Rx is lower noise bandwidth and thermal noise. Therefore, using lower-power Rx and Tx, a similar signal-to-noise ratio (SNR) can be achieved. The main advantage of a wideband Rx is in high data rates due to larger bandwidth available. Operation in large bandwidth offers a sufficient frequency range to distinguish the incoming reflected copies of a signal. Hence, their phase shifts are compensated i.e., they can be summed up coherently. This allows to increase the SNR at the Rx and consequently reduce the PL. The opposite situation occurs when we operate with a smaller frequency range. In that case, signal copies are summed up incoherently.

To obtain a large-scale PL model, we compute the received power of each MPC with our RL simulator. Then, intervehicle distances are calculated. The common form of the log-distance power law PL model – a so-called single-slope approximation model – is given by

$$PL(d) = PL_0 + 10nlog(\frac{d}{d_0}) + X_\sigma, \tag{1}$$

where d is the distance between the Tx and Rx; n is the PL exponent; X_σ is the zero-mean Gaussian distributed random variable with the standard deviation σ; d_0 is the reference distance; and PL_0 is the PL at the reference distance.

In practice, the dual-slope model [18], [14] is considered to be more accurate. The dual-slope model is commonly characterized as a piecewise-linear formulation. The calculation for the dual-slope model is described as

$$PL(d) = \begin{cases} PL_0 + 10n_1log(\frac{d}{d_0}) + X_\sigma, & \text{if } d_0 \leq d \leq d_b \\ PL_0 + 10n_1log(\frac{d}{d_0}) + \\ 10n_2log(\frac{d}{d_0}) + X_\sigma, & \text{if } d > d_b, \end{cases} \tag{2}$$

where d_b is the breakpoint distance; n_1 is the PL exponent corresponding to the PL before the breakpoint; and n_2 is the PL exponent corresponding to the PL after the breakpoint.

We consider d_b as the distance at which the first Fresnel zone touches the ground, or where the first ground reflection traveled $d_b + \lambda/4$ to reach the Rx [14], where λ is the wavelength. In our case, the antenna height is $h_{TX} = h_{RX} = 0.35$ m. Then, one can calculate the breakpoint distance as

$$d_b = \frac{4h_{TX}h_{RX} - \lambda^2/4}{\lambda}. \tag{3}$$

The breakpoint distance is a critical distance at which the PL exponent and the standard deviation are changed drastically.

Further, we use the single-slope approximation model to obtain the PL exponent n and the standard deviation σ in the LoS conditions due to smaller scattering of points. The dual-slope approximation model is utilized to produce the PL exponents n_1, n_2 and the standard deviations σ_1, σ_2 for the non-LoS (NLoS) conditions. It should also be noted that in our approximations we use the floating intercept (FI) model, which implies the least-square linear regression fit. According to the FI model, the values of PL_0 and n are chosen as a result of such fitting.

B. RMS Delay Spread

The RMS delay spread is the second central moment of the channel impulse response. In other words, this is the second central moment of the power-delay-profile (PDP). Mathematically, it can be described by the following equation [11]:

$$\tau_{rms} = \sqrt{\bar{\tau^2} - \bar{\tau}^2}. \tag{4}$$

For L propagation paths, it holds

$$\bar{\tau^n} = \frac{\sum_{i=1}^{L} \tau_i^2 |P_i|^2}{\sum_{i=1}^{L} |P_i|^2}, \tag{5}$$

where P_i is the power of *i*-th propagation path.

C. Angular Spread

We consider both AoA and AoD azimuth spreads. Formally, they are expressed with the following equation [11]:

$$\phi(t) = \sqrt{\sum_l |exp(j\phi_l - (\sum_l (exp(\phi_l, t))))|^2 P_{ang}(\phi_l, t)}, \tag{6}$$

where ϕ_l is the angle of l-th path, and

$$P_{ang}(\phi_l, t) = \sum_\theta \sum_{i=1}^{L} P_{ang}(\phi, \theta, t, \tau_i), \tag{7}$$

where θ is the elevation angle. We only consider the azimuth components of each MPC, because the distribution of their elevation components does not change significantly as compared to the distribution of the azimuth components.

IV. Numerical Results

A summary of the results obtained during our simulations is presented in Table II. A large deviation of the parameters is caused by the variation of distances from 1 to more than 500 meters. First, let us denote the breakpoint distances for the dual-slope approximation. In the case of 28 GHz, the wavelength $\lambda = 0.0107$ m and therefore $d_b = 45.8$ m. In the case of 72 GHz, the wavelength $\lambda = 0.0042$ m and thus $d_b = 117.7$ m. To provide a better fit for the data, it was however shifted to 55 m. The results of the PL modeling are shown in Fig. 3.

In the case of narrow bandwidth and 28 GHz, PL exponents for the low density and for the high density of vehicles are n = 2.36 and n = 2.3 for the LoS links. For the NLoS links, we used the dual-slope approximation; hence, n_1 = 1.21 and n_2 = 3.23 correspond to a low-dense scenario at 28 GHz. The values of n_1 = 1.12 and n_2 = 4.02 correspond to a high-dense scenario at 28 GHz. PL exponents at 72 GHz for low-dense and high-dense scenarios are n = 2.18 and n = 2.17 for the

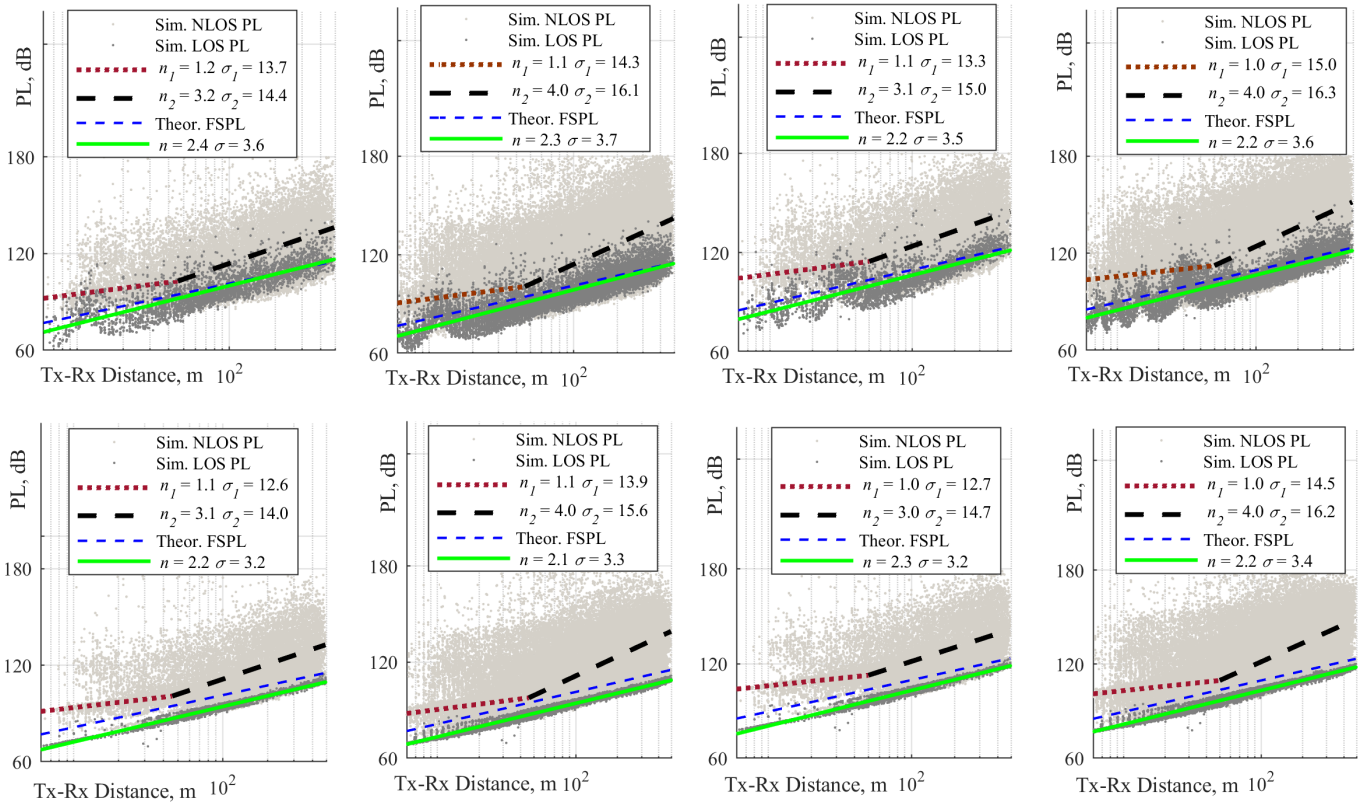

Fig. 3. The results of our PL simulations. The PL in narrowband Rx is represented by the top row of the figures and the PL in wideband Rx is represented by the bottom row of the figures. The first and the second figures of the row represent the PL for 28 GHz (1 - Low Density; 2 - High Density). The third and the fourth figures of the row represent the PL for 72 GHz (3 - Low Density; 4 - High Density).

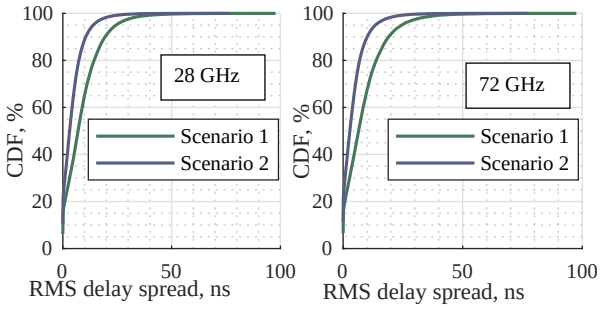

Fig. 4. 28 GHz and 72 GHz RMS delay spread.

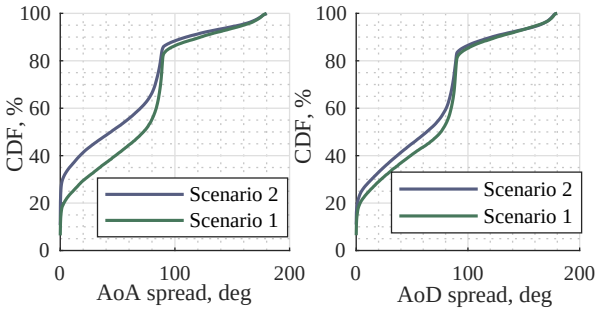

Fig. 5. CDF of AoA spread (left) and AoD spread (right) at 28 GHz.

LoS links. For NLoS at 72 GHz, the PL exponents are n_1 = 1.11, and n_2 = 3.06 for a low-dense scenario and n_1 = 0.95, n_2 = 3.97 for a high-dense scenario.

It should be noted that the coherent summation of MPCs reduces the PL deviation. Hence, for all the cases considered, the PL exponent deviation increases by 0.5 to 1 for the coherent summation. If we consider wide bandwidth at 28 GHz, the PL exponents are n = 2.19 for a low-dense scenario and n = 2.09 for a high-dense scenario for the LoS links. In the case of NLoS, n_1 = 1.08, n_2 = 3.10 for the low-dense deployment and n_1 = 1.10, n_2 = 4.04 for the high-dense deployment. The PL exponents at 72 GHz carrier frequency for low-dense and for high-dense scenarios are n = 2.26 and n = 2.16, respectively, for the LoS links. For the NLoS links at 72 GHz, the PL exponents are n_1 = 0.95, n_2 = 2.92 for the low-dense scenario and n_1 = 0.93, n_2 = 3.95 for the high-dense scenario.

Fig. 4 shows the cumulative distribution function (CDF) of the RMS delay spread at 28 GHz and 72 GHz. This figure includes the CDFs for the first and the second scenarios. The

TABLE II
SUMMARY OF OUR RESULTS

Carrier Frequency	Scenario	Parameter	Value	
			LoS	NLoS
28 GHz	Low Density	PL exponent (n; σ)	(2.36; 3.61)	(1.21; 13.71), (3.22; 14.43)
		RMS delay spread (μ; σ)	(92.67 ns; 84.85 ns)	
		AoA spread (μ; σ)	(61.58; 48.19)	
		AoD spread (μ; σ)	(62.87; 48.94)	
	High Density	PL exponent (n; σ)	(2.3; 3.72)	(1.12; 14.34), (4.02; 16.12)
		RMS delay spread (μ; σ)	(51 ns; 49.37 ns)	
		AoA spread (μ; σ)	(50.30; 49.25)	
		AoD spread (μ; σ)	(58.07; 49.46)	
72 GHz	Low Density	PL exponent (n; σ)	(2.18; 3.51)	(1.11; 13.34), (3.06; 14.98)
		RMS delay spread (μ; σ)	(89.49 ns; 85.58 ns)	
		AoA spread (μ; σ)	(59.42; 47.49)	
		AoD spread (μ; σ)	(60.94; 48.14)	
	High Density	PL exponent (n; σ)	(2.18; 3.61)	(0.95; 14.97), (3.97; 16.31)
		RMS delay spread (μ; σ)	(50.71 ns, 46.95 ns)	
		AoA spread (μ; σ)	(48.52; 48.11)	
		AoD spread (μ; σ)	(55.99; 48.92)	

mean values of the RMS delay spread are μ = 92.67 ns with the standard deviation of σ = 84.85 ns for the low-dense scenario and μ = 51.52 ns with the standard deviation of σ = 49.37 ns for the high-dense scenario at 28 GHz carrier frequency. For 72 GHz carrier frequency, the mean values are μ = 89.49 ns with the standard deviation of σ = 85.58 ns for the low-dense scenario and μ = 50.71 ns with the standard deviation of σ = 46.95 ns for the high-dense scenario.

We calculate the angular spread values for both AoA and AoD. Fig. 5 demonstrates the CDF of AoA and AoD for the carrier frequency of 28 GHz. The behavior of the CDF at 72 GHz is similar to that at 28 GHz. We also compute the mean values of AoA and AoD spreads together with their standard deviations. For the AoD, these values are μ = 62.87, σ = 48.94 and μ = 58.07, σ = 49.46 at 28 GHz for the low-dense and high-dense scenarios, respectively. The AoD spread values at 72 GHz are μ = 60.94, σ = 48.14 for the low-dense scenario and μ = 55.99, σ = 48.92 for the high-dense scenario.

For the AoA CDF, μ = 61.58, σ = 48.19 and μ = 50.30, σ = 49.25 correspond to the low-dense and high-dense scenarios at 28 GHz. The AoA spread values at 72 GHz carrier frequency are μ = 59.42, σ = 47.49 and μ = 48.52, σ = 48.11 for the low-dense and the high-dense scenarios. It can be seen in the figures that all of the CDFs have a sharp 'jump' at around 90 degrees. This phenomenon means that the vast majority of the AoA and AoD angles are close to 90 degrees. However, there are also many other angles having near-zero values, which make a significant contribution to the mean value of the AoA and AoD spreads, thus reducing it. There is no major difference between the low and the high density in terms of the angular spread. The direction spread is higher in more cluttered scenarios because of the congested surroundings.

V. COMPARISON AND DISCUSSION

To validate our findings, we compare them with the reference results for microwave frequencies. The reference data for our comparison are shown in Table III. Measurements in the work [13] were carried out via a channel sounder at 5 GHz with 20 ns delay resolution in different cities and highways of Ohio. The intervehicle distances in question ranged from a few meters to 100 meters in the cities and from a few meters to 1 kilometer on the highways. We focus on the RMS delay spread results for highways with low and high traffic densities because these conditions are most similar to our scenarios. As can be seen in Table III, the overall delay spread is lower in the mmWave frequency range than in the microwave band.

In [17], measurements were conducted for different environments in 5.2 GHz band, and we chose the closest ones to our scenario. In [18] and [14], the dual-slope approximation was used for fitting the measured data. The LoS measurements in [8] were carried out at 2.3 GHz and 5.25 GHz. The antennas were installed on the rooftops of the cars. To be more precise with our simulation results, we consider a higher frequency of 5.25 GHz. In the LoS conditions, the PL exponent in mmWave range is not much higher than in microwave band. This is because the PL exponent tends to the FSPL value, which is equal to 2. With regards to the NLoS conditions, the PL exponent significantly increases due to the link blockage. As for the PL vs. the carrier frequency, the difference between 28 GHz and 72 GHz bands is approximately 3 dB.

Only the AoA measurements in the band of 5.3 GHz with the bandwidth of 60 MHz are considered in [16] due to a small number of Tx elements. It should be noted here that the results in Table III are normalized. It was reported in [16] that high angular spreads of 100 and 290 degrees were obtained due to the reflections from roadside scatterers or vehicles in both the LoS and NLoS cases. The authors of [16] also concluded that the value of the angular delay spread depends mostly on the width of the road. That might be the case, because if we normalize our values, they will be reasonably close to those obtained in [16]. The measurement results similar to our modeling of the angular spread at 5.25 GHz were reported by the METIS project [8].

In summary, our comparison did not reveal dramatically large differences between the results for microwave band and mmWave band, especially in terms of the RMS delay spread

TABLE III
REFERENCE RESULTS

Carrier Frequency	Parameter	Value		Ref.
		LoS	NLoS	
5 GHz	RMS delay spread (High Traffic)	126 ns		[13]
	RMS delay spread (Low Traffic)	53.2 ns		
5.25 GHz	Angular delay spread (mean)	42.7	39.8	
	PL exponent	1. 8	-	[8]
5.2 GHz	PL exponent	1.77	-	[17]
5.6 GHz	PL exponent (n_1, n_2, σ)	(1.81, 2.85, 4.15)	(1.93, 2.74, 6.67)	[14]
5.9 GHz	PL exponent (n_1, σ_1); (n_2, σ_2)	(2, 5.6); (4, 8.4)		[18]
5.8 GHz	RMS delay spread (mean, std)	(59.83 ns, 30.37 ns)	(134.6 ns, 121.9 ns)	[15]
5.3 GHz	Angular delay spread (mean, std)	(0.13, 0.13)	(0.14, 0.15)	[16]

and angular spread. The highest discrepancy was observed for the PL exponents in the NLoS cases due to a difference between propagation properties in the mmWave and the microwave range. The effect of signal blockage has a greater impact on the propagation features in mmWave band, but the presence of a direct path is beneficial. Hence, the absolute difference between the two wave ranges for the RMS delay spread and the angular spread is relatively small.

VI. CONCLUSION

In this paper, we presented a ray-based modeling for V2V mmWave channels considering two carrier frequencies, 28 GHz and 72 GHz, as well as two highway scenarios with low and high densities of vehicles. The main characteristics, such as PL, RMS delay, and angular spread, were obtained for this setup. The actual numerical values of the listed parameters were presented in Table II, which might be useful for further channel modeling. Our simulation results can be considered reliable as they were also compared with previous works to demonstrate adequate convergence. Small discrepancies are caused, primarily, by different frequencies addressed in the previous publications.

REFERENCES

[1] World Health Organization, "Global status report on road safety 2018," tech. rep., World Health Organization, 2018.

[2] R. I. Ansari, C. Chrysostomou, S. A. Hassan, M. Guizani, S. Mumtaz, J. Rodriguez, and J. J. Rodrigues, "5G D2D networks: Techniques, challenges, and future prospects," *IEEE Systems Journal*, vol. 12, no. 4, pp. 3970–3984, 2018.

[3] E. Uhlemann, "Initial steps toward a cellular vehicle-to-everything standard [connected vehicles]," *IEEE Vehicular Technology Magazine*, vol. 12, no. 1, pp. 14–19, 2017.

[4] A. I. Sulyman, A. Alwarafy, G. R. MacCartney, T. S. Rappaport, and A. Alsanie, "Directional radio propagation path loss models for millimeter-wave wireless networks in the 28-, 60-, and 73-GHz bands," *IEEE Transactions on Wireless Communications*, vol. 15, no. 10, pp. 6939–6947, 2016.

[5] M. Boban, D. Dupleich, N. Iqbal, J. Luo, C. Schneider, R. Müller, Z. Yu, D. Steer, T. Jämsä, J. Li, *et al.*, "Multi-band vehicle-to-vehicle channel characterization in the presence of vehicle blockage," *IEEE Access*, vol. 7, pp. 9724–9735, 2019.

[6] J.-J. Park, J. Lee, K.-W. Kim, K.-C. Lee, and M.-D. Kim, "Vehicle antenna position dependent path loss for millimeter-wave V2V communication," in *2018 11th Global Symposium on Millimeter Waves (GSMM)*, pp. 1–3, IEEE, 2018.

[7] E. Kampert, P. A. Jennings, and M. D. Higgins, "Investigating the V2V millimeter-wave channel near a vehicular headlight in an engine bay," *IEEE Communications Letters*, vol. 22, no. 7, pp. 1506–1509, 2018.

[8] L. Raschkowski, P. Kyösti, K. Kusume, T. Jämsä, V. Nurmela, A. Karttunen, A. Roivainen, T. Imai, J. Järveläinen, J. Medbo, J. Vihriälä, J. Meinilä, K. Haneda, V. Hovinen, J. Ylitalo, N. Omaki, A. Hekkala, R. Weiler, and M. Peter, "METIS channel models," 07 2015.

[9] S. Wu, C.-X. Wang, M. M. Alwakeel, X. You, *et al.*, "A general 3-D non-stationary 5G wireless channel model," *IEEE Transactions on Communications*, vol. 66, no. 7, pp. 3065–3078, 2018.

[10] A. Ghazal, Y. Yuan, C.-X. Wang, Y. Zhang, Q. Yao, H. Zhou, and W. Duan, "A non-stationary IM-advanced MIMO channel model for high-mobility wireless communication systems," *IEEE Transactions on Wireless Communications*, vol. 16, no. 4, pp. 2057–2068, 2017.

[11] 3GPP, "Study on channel model for frequencies from 0.5 to 100 GHz," Technical Report (TR) 38.901, 3rd Generation Partnership Project (3GPP), 07 2018. Version 15.0.0.

[12] U.S. Department of Transportation, "Transportation Statistics," annual report, Office of the Secretary of Transportation. Bureau of Transportation Statistics, 2018.

[13] I. Sen and D. W. Matolak, "Vehicle-vehicle channel models for the 5-GHz band," *IEEE Transactions on Intelligent Transportation Systems*, vol. 9, no. 2, pp. 235–245, 2008.

[14] T. Abbas, K. Sjöberg, J. Karedal, and F. Tufvesson, "A measurement based shadow fading model for vehicle-to-vehicle network simulations," *International Journal of Antennas and Propagation*, vol. 2015, 2015.

[15] R. He, A. F. Molisch, F. Tufvesson, Z. Zhong, B. Ai, and T. Zhang, "Vehicle-to-vehicle propagation models with large vehicle obstructions," *IEEE Transactions on Intelligent Transportation Systems*, vol. 15, no. 5, pp. 2237–2248, 2014.

[16] R. He, O. Renaudin, V.-M. Kolmonen, K. Haneda, Z. Zhong, B. Ai, S. Hubert, and C. Oestges, "Vehicle-to-vehicle radio channel characterization in crossroad scenarios.," *IEEE Trans. Vehicular Technology*, vol. 65, no. 8, pp. 5850–5861, 2016.

[17] J. Karedal, N. Czink, A. Paier, F. Tufvesson, and A. F. Molisch, "Path loss modeling for vehicle-to-vehicle communications," *IEEE Transactions on Vehicular Technology*, vol. 60, no. 1, pp. 323–328, 2011.

[18] L. Cheng, B. E. Henty, D. D. Stancil, F. Bai, and P. Mudalige, "Mobile vehicle-to-vehicle narrow-band channel measurement and characterization of the 5.9 GHz dedicated short range communication (DSRC) frequency band," *IEEE Journal on Selected Areas in Communications*, vol. 25, no. 8, 2007.

[19] D. Solomitckii, M. Gapeyenko, V. Semkin, S. Andreev, and Y. Koucheryavy, "Technologies for efficient amateur drone detection in 5G millimeter-wave cellular infrastructure," *IEEE Communications Magazine*, vol. 56, no. 1, pp. 43–50, 2018.

[20] D. Solomitckii, V. Petrov, H. Nikopour, M. Akdeniz, O. Orhan, N. Himayat, S. Talwar, S. Andreev, and Y. Koucheryavy, "Detailed interference analysis in dense mmwave systems employing dual-polarized antennas," in *2017 IEEE Globecom Workshops (GC Wkshps)*, pp. 1–7, IEEE, 2017.

[21] S. Rangan, T. S. Rappaport, and E. Erkip, "Millimeter wave cellular wireless networks: Potentials and challenges," *Proceedings of the IEEE*, vol. 102, no. 3, pp. 366 – 385, 2014.

[22] 3GPP, "Universal Mobile Telecommunications System (UMTS); LTE; 5G; UICC Power Optimisation for Machine-Type Communication (MTC) ," Technical Report (TR) 31.970, 3rd Generation Partnership Project (3GPP), 07 2018. Version 15.0.0.